Hindawi
Mathematical Problems in Engineering
Volume 2018, Article ID 7641862, 18 pages
https://doi.org/10.1155/2018/7641862

Research Article

Speed Control for a Marine Diesel Engine Based on the Combined Linear-Nonlinear Active Disturbance Rejection Control

Runzhi Wang[1], **Xuemin Li**[1], **Jiguang Zhang**[2], **Jian Zhang**[1], **Wenhui Li**[1], **Yufei Liu**[1], **Wenjie Fu**[1] and **Xiuzhen Ma**[1]

[1]*College of Power and Energy Engineering, Harbin Engineering University, Harbin 150001, China*
[2]*China State Shipbuilding Corporation Limited, Beijing 100048, China*

Correspondence should be addressed to Xuemin Li; lxm@hrbeu.edu.cn

Received 23 July 2018; Revised 11 November 2018; Accepted 28 November 2018; Published 13 December 2018

Academic Editor: Luis J. Yebra

In this paper, a compound control scheme with linear active disturbance rejection control (LADRC) and nonlinear active disturbance rejection control (NLADRC) is designed to stabilize the speed control system of the marine engine. To deal with the high nonlinearity and the complex disturbance and noise conditions in marine engines, the advantages of both LADRC and NLADRC are employed. As the extended state observer (ESO) is affected severely by the inherent characteristics (cyclic speed fluctuation, cylinder-to-cylinder deviations, etc.) of the reciprocating engines, a cycle-detailed hybrid nonlinear engine model is adopted to analyze the impact of such characteristics. Hence, the controller can be evaluated based on the modified engine model to achieve more reliable performance. Considering the mentioned natural properties in reciprocating engines, the parameters of linear ESO (LESO), nonlinear ESO (NLESO), and the switching strategy between LADRC and NLADRC are designed. Finally, various comparative simulations are carried out to show the effectiveness of the proposed control scheme and the superiority of switching strategy. The simulation results demonstrate that the proposed control scheme has prominent control effects both under the speed tracking mode and the condition with different types and levels of load disturbance. This study also reveals that when ADRC related approaches are employed to the reciprocating engine, the impact of the inherent characteristics of such engine on the ESO should be considered well.

1. Introduction

Compared with the aviation, rail, and automobile transport, shipping is known as the most energy efficient and environmental friendly classical mode of transport [1]. The energy generated by marine diesel engines is widely used in the domain of ship propulsion [2–5]. In such application, speed control for the marine main engine becomes a crucial task.

On the one hand, the engine speed should be regulated effectively over all working points of the engine. Otherwise, the oscillation of engine speed would lead to abnormal operating conditions [4], which decreases the service life of engines and even results in premature failure of the transmission system in case of severe speed fluctuation [6]. Moreover, sustained overspeed will cause irreversible damage to the marine main engine [7]. On the other, an excellent speed controller can help the engine keep good power performance under its complex operation conditions, thus reducing the fuel consumption and emission [8, 9] and releasing partial burden of the engine control unit (ECU) from the increasingly strict diesel emission regulations.

The main task of marine engine speed control comprises tracking the target speed fast and maintaining the engine speed steady in the presence of the intrinsic instabilities and disturbances coupled with the fast and dynamic changes of external environment, load, and operation conditions [7].

Historically, various different strategies have been adopted on the speed regulation for marine main engines, such as traditional PID [10], sliding mode control (SMC) [3], H_∞ control [11], fuzzy control [7], and model predictive

control (MPC) [12]. Although these control strategies have been attempted to provide feasible ways to deal with the marine engine speed control issue, most of them have corresponding drawbacks. For instance, the parameters in classical PID need to be readjusted when the engine operation deviates further from the calibrated situation caused by the changing of external condition; the chattering phenomenon in SMC is hard to be eliminated; the control effect of H_∞ and fuzzy methods is limited because the operation condition of the marine engine varies widely; and the implementation of MPC is complex and with considerable high cost.

So far, speed regulation for diesel engines remains to be a challengeable mission due to the fact that diesel engines are inherently high nonlinear, and their load disturbance is harsh and unpredictable. In fact, the load disturbance not only varies with the operation condition but also is affected strongly by numerous other external aspects, such as the marine weather and the sea surface condition [3, 13]. In the moderate sea conditions, the load disturbance is mainly caused by ocean current. However, when a ship navigates in extreme seas, partial or whole, the propeller disk would emerge from the water. Hence, different levels of change in propeller torque might exist and would result in a large fluctuation in marine engine speed [14].

Focusing on the mentioned sophisticated load disturbance, active disturbance rejection control (ADRC) has been applied to the marine engine speed control because of its considerable control effect in dealing with the system with uncertain disturbances. It has been proved by enormous practical applications in extensive industrial domains, such as in [15–18], that ADRC has strong robustness towards parameters variations, disturbances, and noises. In the field of marine main engine, for instance, in [19], a nonlinear active disturbance rejection controller was designed for a MAN B&W large low-speed diesel engine via a simplified transfer function engine model. In [20], a combined controller based on cerebellar model articulation controller (CMAC) and ADRC was presented to control the engine speed on a simplified empirical diesel engine model coupled with the model of propeller and hull dynamics.

However, in most of the previous articles concerning marine engine speed control, the controllers were only evaluated by using simple engine models. The impact of the intrinsical characteristic of the engine speed on the control effect of these controllers has been ignored. In terms of the reciprocating engine, engine speed is naturally cyclic fluctuation due to the existence of the in-cylinder discrete torque generation [21, 22]. The periodic instant speed signal in the crank-angle (CA) domain is cyclic but aperiodic in the time domain as the engine speed varies [23]. The inherent speed fluctuation would be more serious when affected by cylinder-to-cylinder and cycle-to-cycle differences in torque production [21, 24]. Furthermore, the deviations in engine speed caused by imbalance working in cylinders are characterized as periodic disturbances in the CA domain [21] rather than the general time domain, which has been proved as a difficulty for asymptotic tracking and disturbance rejection [23]. In this study, it is found that this phenomenon has a significant impact on the performance of the ESO.

In general, it is reported that the mean value engine model (MVEM) is sufficient for controller design [25, 26]. But for some control algorithms it can be summed up from previous articles that it is hard to guarantee the objectivity when designing a speed controller for the reciprocating engine, because of the existence of these ignored characteristics in engine speed. For example, as for SMC, there are papers researched the application by testing MVEM or else simplified engine model, and the results are found to be satisfactory [3, 27]. Nevertheless, when the similar methods were tested on a more complex engine model or a real engine, the results turned out to be less ideal. In [28, 29], the oscillation in speed caused by the coupling of chattering phenomenon in SMC and the inherent speed fluctuation in reciprocating engine cannot be alleviated easily, and the oscillation of control input is also apparent [27]. Likewise, this is also an inevitable impact for the controller based on ADRC as the control performance of ADRC is affected by noise and disturbance [17, 30].

It should be pointed out that the mentioned issue has not drawn any attention when the ADRC method is applied on the engine speed regulation, whereas its impact can be observed in related articles. In [8], a linear ADRC (LADRC) framework was adopted to compensate the total disturbance for idle speed control in a diesel engine. Although the control performance for sudden load disturbances has been improved effectively, the steady-state speed variation is obviously larger than it in the commercial controller where PID method is employed. As far as the authors know, there is no analysis about the reason therein.

As mentioned above, the noise and disturbance are extremely complex and uncertain in marine engines, and the type and extent of the disturbance are various. Moreover, the performance of ESO is also affected by the natural speed fluctuation. Single LADRC or nonlinear ADRC (NLADRC) may not guarantee control performance over the whole work conditions. In [31], a systemic analysis of the characteristics of LADRC and NLADRC is provided. Normally, NLADRC outperforms LADRC, but when the level of the total noise and disturbance turns to a certain degree, the performance of NLADRC will decrease sharply [31]. It is summarized that by combining LADRC and NLADRC, it leads to a better method called LADRC/NLADRC switching control (SADRC), which keeps the merits of both methods. Better control performance can be obtained when the total disturbance and noise are complicated, and their amplitudes change widely. This kind of control strategy has not been tested in marine engine speed control domain which suffered from the mentioned sophisticated load disturbance, noise, and the inherent speed fluctuation.

Motivated by the previous research and the challenges stated above, a speed controller that employs the SADRC scheme is designed to deal with the complex noise and disturbance in the marine engine. Considering the analysis above about the inadequacy in the validation of the previous ADRC based controllers for the diesel engine speed control via MVEMs or simpler engine models, a more detailed engine

model is adopted, which can exhibit the inherent speed fluctuation. Aiming at the special features of the engine speed, the parameters for the proposed controller are adjusted via analyzing the impact of the inherent speed fluctuation on the performance of ESO. Finally, in order to show the superiority of the proposed scheme, comparisons between the proposed control scheme and other controllers are carried out under speed tracking mode and various external load disturbance conditions.

The rest of this paper is organized as follows. A cycle-detailed hybrid nonlinear engine model is presented in Section 2, and the detailed differences between the proposed engine model and the classic MVEM are compared. In Section 3, the SADRC algorithm for engine speed control is described. And the impact of the inherent speed fluctuation on the performance of ESO is studied, based on which the parameters in the proposed controller are designed. Section 4 exhibits the control performance of the proposed controller by comparing with LADRC, NLADRC, and PID controller. In Section 5, the conclusion is summarized about the whole work in this study, and a research direction for further work is discussed.

2. The Cycle-Detailed Hybrid Nonlinear Engine Model

In this study, the idea in [22, 32] is employed to modify the common MVEM. By doing such, the advantages in the MVEM are kept; meanwhile, the inherent speed fluctuation caused by the discrete torque generation and cyclic deviations among cylinders can be simulated without making the engine model more complex and harder to be executed in computation. Figure 1 demonstrates the thermodynamic volumes for the marine engine. The engine model is composed of five parts which are the intake and exhaust manifold, cylinders, intercooler, and turbocharger. In this paper, only the discrete torque generation process and the final crankshaft dynamic are provided. Else contents of the engine model, such as engine cycle delays, intake and exhaust manifold, intercooler, turbocharger, can refer to the authors' previous work [5].

2.1. The Discrete Torque Generation Process. The CA signal φ is calculated by

$$\varphi = \mathrm{mod}\left(\int 6n_e dt, 720\right), \tag{1}$$

where n_e is engine speed and operator "mod" represents modulus.

Such CA signal is used to decide the timing sequence for the in-cylinder process. For the individual cylinder, the discrete torque generation mechanism and the in-cylinder evolution process can be shown in the form of finite-state machines (FSMs) [22, 32]. Figure 2 shows that the indicated torque is produced only within the phases "C" to "E". Assuming the indicated torque is sustained unchanged during such phase, the mean indicated torque value in the whole working cycle can be replaced by the mean indicated torque during the process from "C" to "E".

Moreover, to simulate the imbalance working ability among cylinders, a factor ξ_i is defined, which denotes the cylinder-by-cylinder variation of the cylinder i. As a result, the gross indicated torque M_{ig}^i for the cylinder i is shown as follows

$$M_{ig}^i = P_{durtion} \frac{30 \cdot W_f^i \cdot q_{HV} \cdot \eta_{ig}^i}{\pi \cdot n_e} \frac{720}{N_c \cdot \varphi_F} \xi_i, \tag{2}$$

$$P_{durtion} = \begin{cases} 1 & (i-1)\dfrac{360}{N_c} < \varphi < (i-1)\dfrac{360}{N_c} + \varphi_f \\ 0 & otherwise, \end{cases} \tag{3}$$

$$\eta_{ig}^i = f\left(n_e, \lambda^i\right), \tag{4}$$

where $P_{durtion}$ is pulse function, W_f^i is the fuel mass flow rate of the cylinder i, q_{HV} is the low calorific value of diesel, η_{ig}^i represents the indicated efficiency of the cylinder i, which can be defined as a function between the engine speed and air to fuel ratio (AFR) (defined as λ^i for the cylinder i), φ_f means the lasting angle of the expansion phase, and N_c is the number of cylinders.

The mass fuel flow of the cylinder i, W_f^i, can be calculated by

$$W_f^i = \frac{n_e \cdot N_c \cdot m_f}{120} \cdot 10^{-6}, \tag{5}$$

where m_f is the control input (fuel injection quality per stroke per cylinder).

The total gross indicated torque M_{ig} is

$$M_{ig} = \sum_1^{N_c} M_{ig}^i. \tag{6}$$

2.2. Engine Rotational Dynamic. Combing the indicated torque from all cylinders, the engine rotational dynamic equation can be described by

$$J_e \frac{dn_e}{dt} = \frac{30}{\pi}\left(M_{ig} - \left(M_p + M_f + M_{load} + M_{wave} + M_{noise}\right)\right), \tag{7}$$

where J_e is the total rotary inertia, M_p is the pumping torque, M_f is the friction torque, M_{load} means the load torque, M_{wave} represents the load disturbance from wave, and M_{noise} is the total bounded disturbance.

For more information about the engine model and the mentioned symbols, refer to [5].

2.3. The Comparison between the Cycle-Detailed Hybrid Nonlinear Engine Model and the MVEM. Under the same control parameters (a PID controller), noise condition, and tested

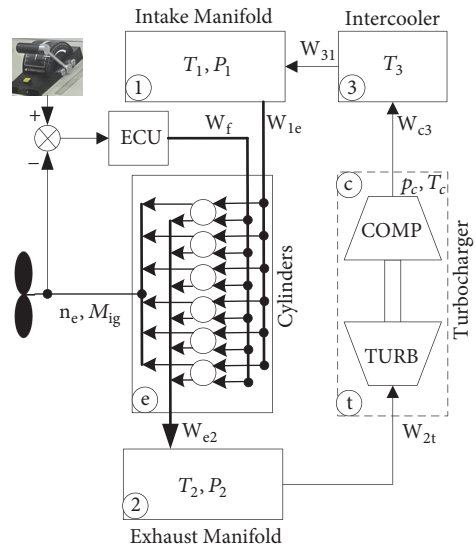

Figure 1: Schematic diagram of the marine diesel engine for propulsion.

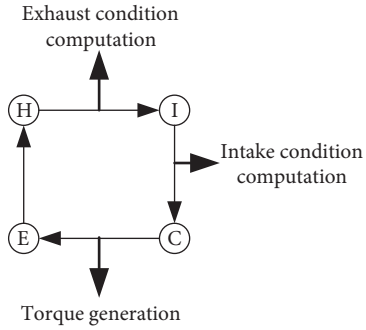

Figure 2: In-cylinder evolution process (where "I" represents intake process, "C" compression process, "E" expansion process, and "H" exhaust process).

process, the individual cylinder indicted torque waveform of the hybrid engine model can be demonstrated in Figure 3(a). The comparisons of the total indicated torque and the engine speed for both engine models are shown in Figures 3(b) and 3(c), respectively. The right side of Figure 3 denotes the enlarged plots for the corresponding compared variables within around one engine working cycle.

Figure 3(a) shows the pulse indicated torque in individual cylinder. It can clearly illustrate the discrete torque generation process. Meanwhile, it can be known from Figure 3(b) that the mean effect of the total indicated torque in the proposed engine model is almost the same in MVEM. It can be observed from Figure 3(c) that the inherent speed fluctuation can be modeled in the proposed engine model. The engine speed fluctuation (instant and average speed) in the engine model is significantly larger than that in the MVEM. And the control effect in the proposed engine model is inferior to that in the MVEM. Note that the MVEM has been verified in authors' previous research [3]. It can be noticed from Figure 3(c) that the speed responses in the two models are the same in overall, which can be believed as the verification of the proposed model in this study.

3. Controller Design

3.1. Basic Description of the ADRC. It was proved in previous papers, such as [8, 19, 20], that second-order or even first-order ADRC is suitable to the engine speed control by some corresponding simplifications. To improve the speed control accuracy, we decide to adopt second-order ADRC, although the engine rotational dynamic model Equation (7) is first-order. On one hand, having the engine system with inevitable delay (such as turbocharge lag and cyclic combustion delay), the first-order ADRC would not guarantee control performance in some working conditions. On the other, the second-order ADRC has better adaptability and disturbance prediction ability [33], which will improve the control performance in the case of sophisticated working conditions for marine diesel engines. In order to show clearly the advantage of the using second-order ADRC, Figure 4 gives the control performance comparison between them. It is obvious that the overshoot, settling time, and the steady-state speed fluctuation in the former are larger than those in the latter.

Taking the derivative of both sides of (7), we can get

$$\ddot{n}_e = \frac{30}{\pi J_e}\dot{M}_{ig} - f\left(n_e, \dot{n}_e, \lambda^i, \omega(t)\right) \tag{8}$$

where $\dot{n}_e$ is the derivate of engine speed n_e, $\omega(t)$ means the unknown disturbance and unmodeled dynamics, $f(n_e, \dot{n}_e, \lambda^i, \omega(t)) = 30(\dot{M}_p + \dot{M}_f + \dot{M}_{load} + \dot{M}_{noise} + \dot{M}_{wave})/\pi J_e$,

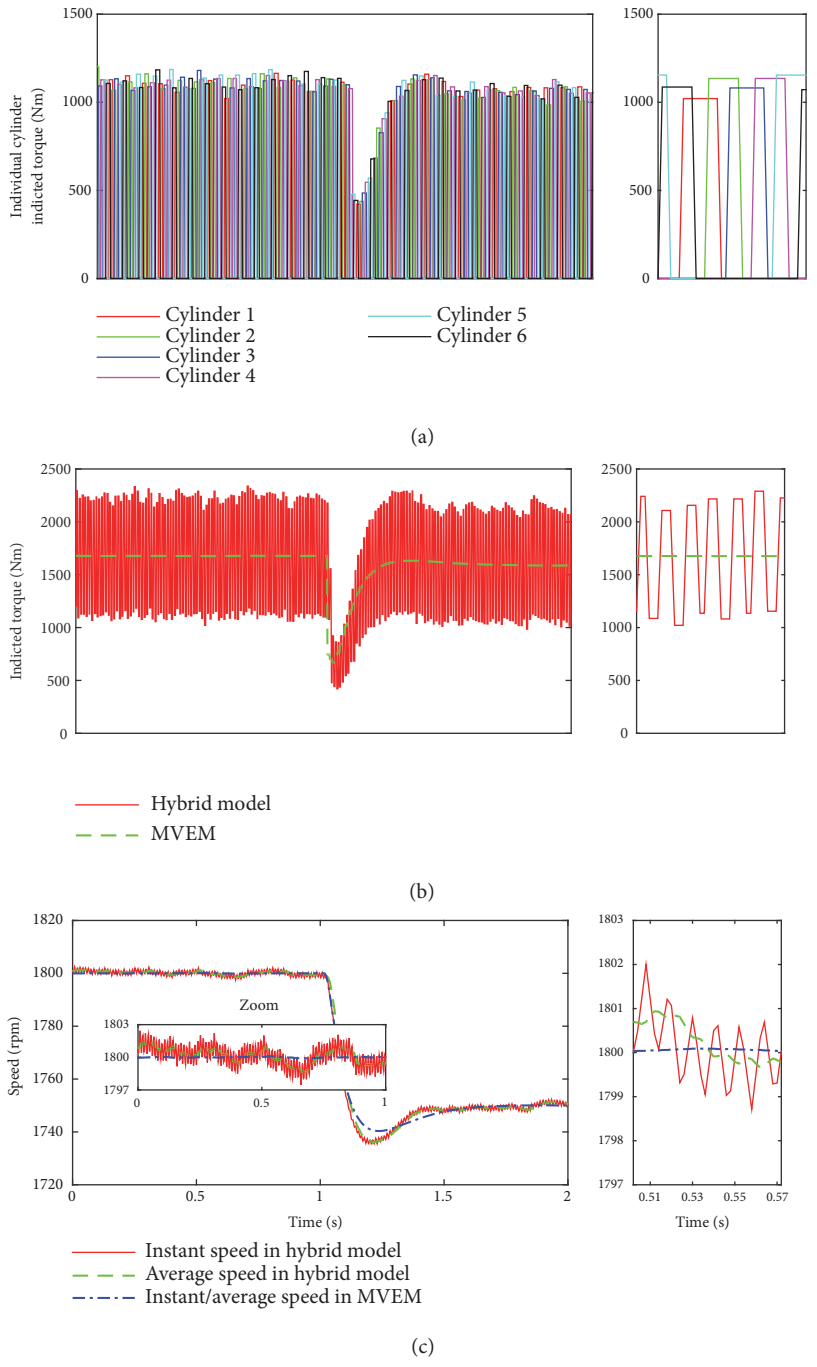

Figure 3: The comparisons of both engine models. (a) Individual cylinder indicated torque in the proposed engine model. (b) Total indicated torque of both engine models. (c) The speed responses of both engine models.

is an unknown and time-varying function, and $\dot{M}_{ig}$ can be written as

$$\dot{M}_{ig} = \sum_{1}^{N_c} \dot{M}_{ig}^{i} = K \cdot g\left(n_e, \dot{n}_e, \lambda^i\right) \cdot \dot{m}_f \tag{9}$$

where $K = (180 q_{HV} \xi_i / \pi \varphi_F J_e) 10^{-6}$, $g(n_e, \dot{n}_e, \lambda^i) \cdot \dot{m}_f = \sum_1^{N_c} (d(P_{durtion}(n_e) \cdot \eta_{ig}^i(n_e, \lambda^i) \cdot m_f)/dt)$ is a nonlinear time-varying function and $\dot{m}_f$ is an intermediate variable without practical significance.

Combining (8) and (9), a new second-order dynamic model for engine speed can be constructed as follows

$$\begin{aligned} \ddot{n}_e &= K \cdot g\left(n_e, \dot{n}_e, \lambda^i\right) \cdot \dot{m}_f - f\left(n_e, \dot{n}_e, \lambda^i, \omega(t)\right) \\ &= b(t) \cdot m_f - f\left(n_e, \dot{n}_e, \lambda^i, \omega(t)\right), \end{aligned} \tag{10}$$

where $b(t) = (30K \cdot g(n_e, \dot{n}_e, \lambda^i) \cdot \dot{m}_f)/\pi J_e m_f$.

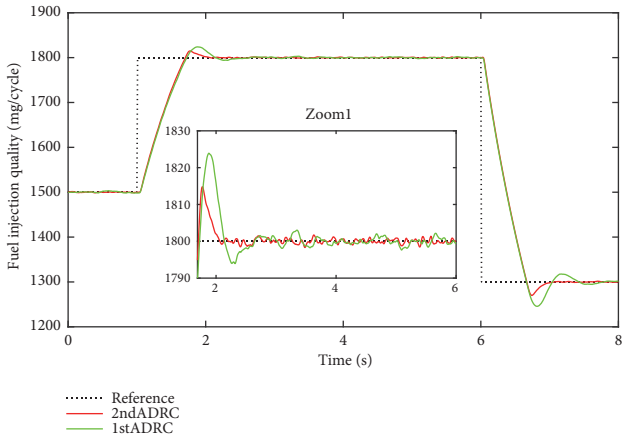

FIGURE 4: The control performance comparison between first-order and second-order ADRC.

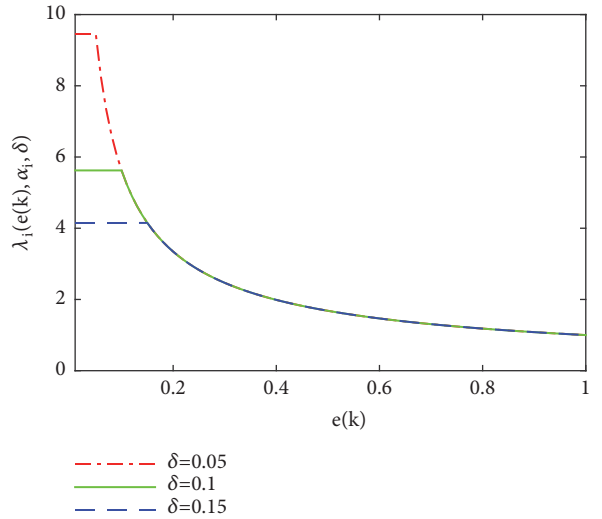

FIGURE 5: Demonstration of the function $\lambda_i(e(k), \alpha_i, \delta)$ when $\alpha = 0.25$.

Defining $x_1 = n_e$, $x_2 = \dot{n}_e$, $x_3 = f(n_e, \dot{n}_e, \lambda^i, \omega(t))$, $u = m_f$, (10) can be rewritten in the form of state-space as follows

$$\begin{aligned} \dot{x}_1 &= x_2 \\ \dot{x}_2 &= b(t)\, u - x_3 \\ \dot{x}_3 &= \dot{f}\left(n_e, \dot{n}_e, \lambda^i, \omega(t)\right) \\ y &= x_1 \end{aligned} \tag{11}$$

where x_3 represents the nonlinear dynamics of the engine, including the total lumped disturbance.

Hence, focusing on the state-space Equation (11), we study the second-order ADRC for diesel engine speed control in this study. According to [34], a general third-order ESO for the second-order system Equation (11) can be given as

$$\begin{aligned} e(k) &= z_1(k) - y \\ z_1(k+1) &= z_1(k) + h\left(z_2(k) - \beta_{01}\varphi_1(e(k))\right) \\ z_2(k+1) &= z_2(k) \\ &\quad + h\left(b_0 u(k) + z_3(k) - \beta_{02}\varphi_2(e(k))\right) \\ z_3(k+1) &= z_3(k) - h\beta_{03}\varphi_3(e(k)) \end{aligned} \tag{12}$$

where y is the system output, h is step size, $u(k)$ is the control input at instant k, b_0 is the control gain, β_{0i} $(i=1,2,3)$ are the gains of observer, $z_1(k)$ and $z_2(k)$ are the estimation of the system states at the instant k, $z_3(k)$ is the estimation of the total disturbance at the instant k, and $\varphi_i(e(k))$ $(i=1,2,3)$ are nonlinear functions, which can be defined as

$$\begin{aligned} \varphi_i(e(k)) &= fal\left(e(k), \alpha_i, \delta\right) \\ &= \begin{cases} \dfrac{e(k)}{\delta^{1-\alpha_i}} & |e(k)| \le \delta \\ |e(k)|^{\alpha_i} \operatorname{sgn}(e(k)) & |e(k)| > \delta \end{cases} \end{aligned} \tag{13}$$

where α_i and δ can be decided in advance; some recommended values are summed up in Han's research [35]. When $\alpha_i < 1$, this function can represent the characteristic of "small error, big gain; big error, small gain". When $\alpha_i = 1$, it becomes a linear function.

To show clearly the effect of "small error, big gain; big error, small gain", according to [31], function $fal(e(k), \alpha_i, \delta)$ can be rewritten as

$$\begin{aligned} fal\left(e(k), \alpha_i, \delta\right) &= \frac{fal\left(e(k), \alpha_i, \delta\right)}{e(k)} e(k) \\ &= \lambda_i\left(e(k), \alpha_i, \delta\right) e(k) \end{aligned} \tag{14}$$

For instance, $\alpha = 0.25$, and taking δ as 0.05, 0.1, and 0.15, respectively, a set of curves for $\lambda_i(e(k), \alpha_i, \delta)$ can be obtained in Figure 5.

Hence, state error feedback control law can be defined as

$$\begin{aligned} e_1 &= v_1(k) - z_1(k) \\ e_2 &= v_2(k) - z_2(k) \\ u_0 &= \beta_1 fal\left(e_1, \alpha_i, \delta\right) + \beta_2 fal\left(e_2, \alpha_i', \delta'\right) \end{aligned} \tag{15}$$

where $v_1(k)$ and $v_2(k)$ are the set-points and their differential at the sampling instant k, respectively, and β_1 and β_2 are the control gains, which can be considered as nonlinear or linear control law based on the value of α_i'.

In this study, to reduce both the amplification effect of noise and the burden of parameters tuning, we adopt linear control law. Hence, the state error feedback control law can be written as

$$u_0 = \beta_1 e_1 + \beta_2 e_2 \tag{16}$$

Considering the disturbance compensation, the control input can be given as

$$u(k) = u_0 - \frac{z_3(k)}{b_0} \tag{17}$$

3.2. Scheme of SADRC for Marine Engine Speed Control. As the state error feedback control law is chosen to be linear, the switching scheme for SADRC refers to the shift between the linear ESO (LESO) and the nonlinear ESO (NLESO).

Motivated by [31], the switch process depends on the value of $e(k)$. We do not consider the transition time as another shift condition as in [31]. Hence, only a specific value e_m should be decided, thus the shift between LESO and NLESO can be completed. To be specific, in the case of $|e(k)| < e_m$, NLESO works; otherwise, LESO takes the place of it. The method for selecting e_m proposed in [31] cannot be used directly in this study. The reason will be explained after introducing the parameters tuning of ESO (see Remark 2).

Given the input saturation of the actuator, the input signal for ESO diverges from the original control input, which causes the inaccurate estimation of the total disturbance in ESO. As shown in [36] and the references therein, a simple solution is to replace the control input for ESO by the saturated value of actuator.

To sum up, we can get the SADRC controller for marine engine speed control as illustrated in Figure 6.

3.3. Parameters Tuning of the SADRC for Marine Engine Speed Control. The parameters tuning in ADRC are sophisticated as there are multiple parameters that need to be adjusted, especially for NLADRC. Gao proposed a tuning method based on observer bandwidth for LADRC [30]. The parameters of LESO can be chosen as

$$\begin{aligned} \beta_{01} &= 3\omega_o, \\ \beta_{02} &= 3\omega_o^2, \\ \beta_{03} &= \omega_o^3, \end{aligned} \tag{18}$$

$$\omega_o = 5\sim 10\omega_c, \tag{19}$$

where ω_o denotes the bandwidth of observer, which has a relationship with the control bandwidth ω_c.

The determination of ω_c can be found in [37], and it can be calculated by

$$\omega_c = \frac{10}{t_s^*} \tag{20}$$

where t_s^* denotes the desired setting time, which can be obtained by practical demand.

Initially, in this study, for the target engine, according to its response time (refering to Figure 4, the settling time for the acceleration and deceleration processes is within the range from 1s to 2s), the desired setting time is set to be 2s, i.e., $t_s^* \approx 2s$. The choice of t_s^* should consider the limitation of the engine, including the mechanical safety and emission; for example, to obtain small t_s^*, the engine needs to run with quick speedup procedure, which would cause incomplete combustion or even damage to engine. Then we can get $\omega_c = 5$ by (20). Choosing $\omega_o = 8\omega_c = 40$, the parameters in LESO can be obtained with the method of (18) Thus, we have $\beta_{01} = 120$, $\beta_{02} = 4800$, $\beta_{03} = 64000$. Note that the variations among cylinders have not been considered firstly, i.e., the factor $\xi_i = 1$.

On the basis of the initial parameters of LESO, the proper control parameters of linear error state feedback (LESF) are decided via trial-and-error approach in the proposed engine model. During such process, we follow some fundamentals: the delay in disturbance estimation depends on β_{03}, the bigger β_{03}, the less delay, but oversize β_{03} leads to oscillation; meanwhile, the control performance can be improved to a certain degree by adjusting β_{01} and β_{02} coordinately. Finally, we get the proper parameters for LESO: $\beta_{01} = 200, \beta_{02} = 10000, \beta_{03} = 60000$, and parameters for LESF: $\beta_1 = 4.5$, $\beta_2 = 0.15$, $b_0 = 500$. The control effect will be given in next section.

As for NLADRC, in [31], empirical formulas are summarized for the parameters design in NLESO. They can be decided as follows

$$\begin{aligned} \beta'_{01} &= 3\omega_o, \\ \beta'_{02} &= \frac{3\omega_o^2}{5}, \\ \beta'_{03} &= \frac{\omega_o^3}{9}. \end{aligned} \tag{21}$$

Remark 1. It is not possible to get feasible parameters to keep stability by (21) in this study. To get suitable parameters for NLESO, the impact of the inherent characteristics of the engine (such as speed fluctuation) on the performance of the ESO needs to be analyzed. But firstly, some parameters can be decided as $\alpha_1 = 1$, $\alpha_2 = 0.5$, $\alpha_3 = 0.25$ by common previous experience [35].

Meanwhile, to illustrate the necessity of taking into account the inherent speed fluctuation while designing ADRC related controller for engine speed control, the estimation performances of the ESO between the proposed engine model and the MVEM are compared in detail. We find it easier to get the parameters of LESO in MVEM. The values calculated directly from (18) are adequate, i.e., $\beta_{01} = 120$, $\beta_{02} = 4800$, $\beta_{03} = 64000$. Moreover, the parameters for LESO in the MVEM have a wider range than those in the proposed engine model.

The tracking curves of LESO state $z_1$and z_2 for both engine models are shown in Figure 7. The tracking performance for z_3 is not given for the total disturbance is unknown. Note that the noise condition is the same in both engine models. Moreover, the sampling and control time are designed to be 0.01s ($h = 0.01$) in both engine models.

It can be observed from Figure 7 that z_1 and z_2 can appropriately track the system states. However, significant differences can be seen between the tracking curves of the two engine models. In the proposed engine model, the bound of the distribution of the tracking error $e(k)$ is $[-1.5, 1.5]$, and most of $e(k)$ distributes in the range $[-1.0, 1.0]$, whereas there is an order of magnitude difference for the corresponding values in the MVEM. Also, the changing frequency of these variables is apparently different in the two engine models. It is higher in the MVEM. The main reason is that the speed or torque changing is cycle based in the proposed engine model, while it is time based in the MVEM. From Figure 7 (c1), (c2),

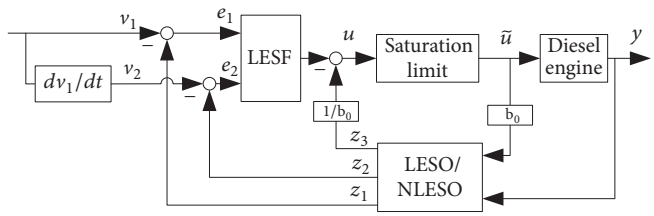

Figure 6: Basic control structure diagram of the SADRC method for marine engine speed control.

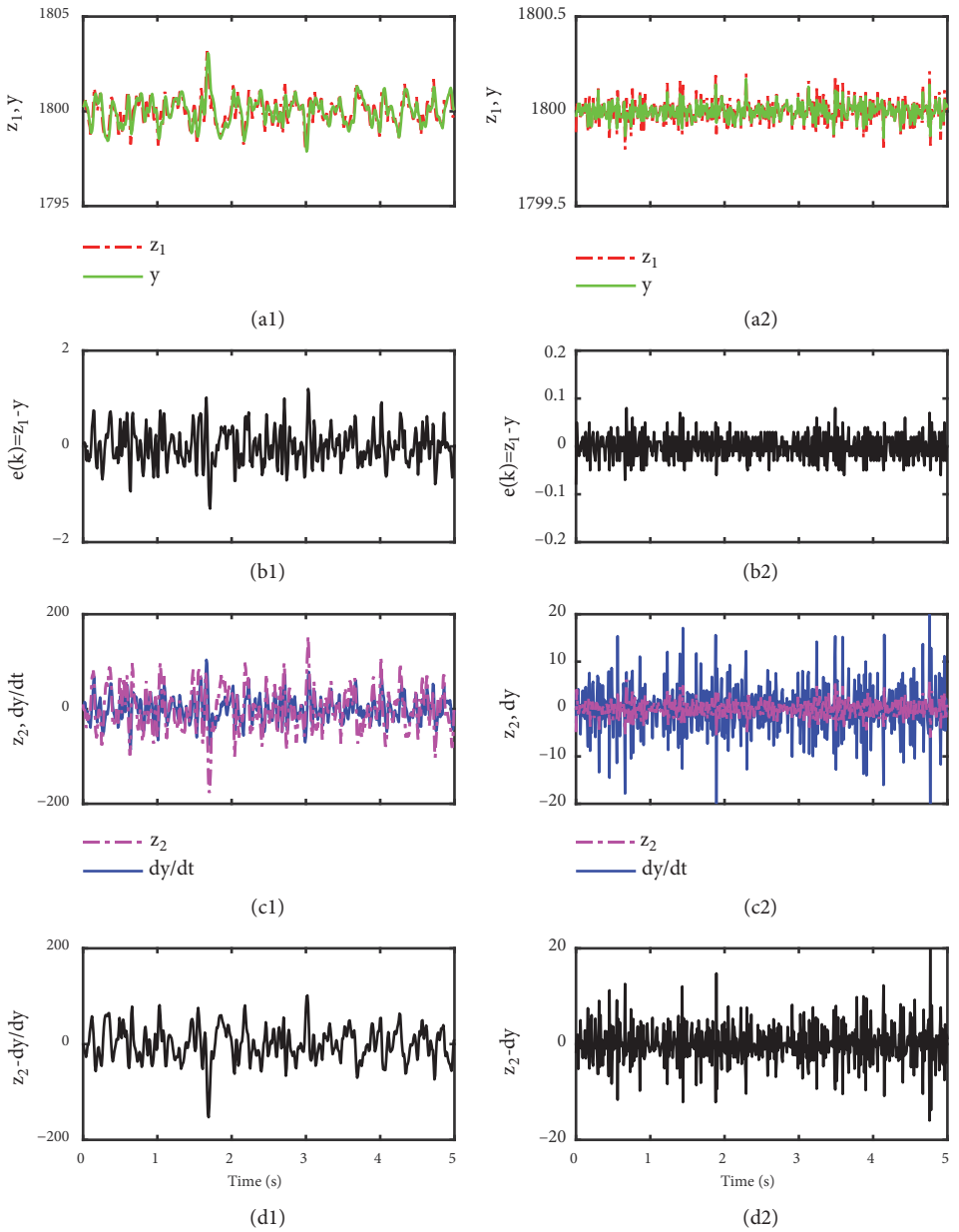

Figure 7: The tracking condition of the LESO state under different engine models. (a1) The tracking curves of z_1 and y in the proposed engine model. (b1) The error between z_1 and y in the proposed engine model. (c1) The tracking curves of z_2 and dy/dt in the proposed engine model. (d1) The error between z_2 and dy/dt in the proposed engine model. (a2), (b2), (c2), and (d2) represent the corresponding variables in the MVEM, respectively.

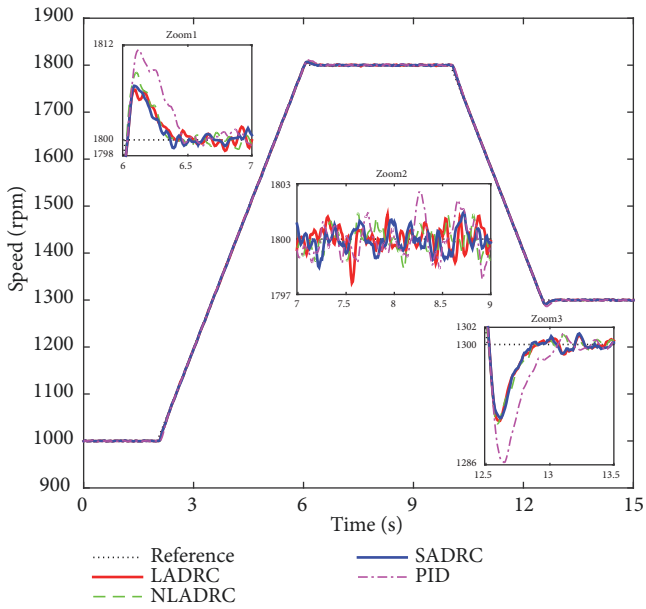

Figure 8: The comparisons of speed tracking performance.

we know that the estimated differential z_2 is more smooth than the time-derivative of y (dy/dt). This means that the LESO can effectively filter the disturbed time-derivative of y then lessen the noise effect on the control performance in the MVEM. On the contrary, this effect is not obvious or weak in the proposed engine model.

Since the tracking performance can hardly be improved by tuning the parameters of LESO in this study, it can be concluded that the performance of ESO (including LESO and NLESO) is limited by the inherent property in speed fluctuation, and the distribution of $e(k)$ mentioned above is a kind of inherent property in reciprocating engines. This is different with other references, such as in [30, 31, 38, 39], where the tracking error $e(k)$ is with a very small distribution range under steady-state. This property cannot be eliminated in the reciprocating engine. Furthermore, in a real engine, when $e(k)$ is affected by the coupled effect of the inherent speed fluctuation and other noise and disturbance, the actual $e(k)$ would far exceed the bound $[-1.0, 1.0]$ inevitably. As a result, the estimating capacity of NLESO would deteriorate sharply, due to the fact shown in Figure 5 that the equivalent gain $\lambda_i(e(k), \alpha_i, \delta) < 1$ when $e(k) > 1$.

Remark 2. Under the background mentioned above, an enlightenment is got for designing the parameters $\beta'_{01}, \beta'_{02}, \beta'_{03}, \delta'$ in NLESO and e_m in SADRC. The basic rule is to avoid excessively amplifying the inherent property in speed fluctuation when $e(k) < 1$, which requires that the nonlinear gains maintain with relatively small value while $e(k) < 1$. Therefore, δ' is chosen to be 0.1 to limit the maximum in gains. Then $\beta'_{01}, \beta'_{02}, \beta'_{03}$ are regulated by reducing the corresponding value in obtained $\beta_{01}, \beta_{02}, \beta_{03}$ (for LESO). Eventually, the proper parameters for NLESO can be determined as $\beta'_{01} = 150, \beta'_{02} = 1200, \beta'_{03} = 5800$. The switching condition is chosen as $e_m = 1$, it means that, on the one hand, the advantage in NLESO is kept when $e(k) < 1$, and, on the other, LESO can avoid the performance degrading in NLESO when $e(k) > 1$. The choice of e_m is based on the characteristics in engine rather than the recommended value in [31]. The rationality to choose $e_m = 1$ as the switching condition also was mentioned in [40].

4. Simulation and Analysis

4.1. Engine Speed Tracking Performance. As it is exhibited in Figure 8, to simulate the real acceleration and deceleration processes in a marine diesel engine for propulsion, ramp references are adopted. And four controllers (LADRC, NLADRC, SADRC, and PID) are compared to prove the superiority of the proposed method. The control parameters of the classical PID are well tuned by trail-and-error scheme with the consideration of wind-up scheme. Note that the load torque is normalized during these processes, and noise load is set as banded white noise with a basic constant 200 N·m. Besides, the cylinder-by-cylinder variation degree is designed as $[\xi_1, \xi_2, \xi_3, \xi_4, \xi_5, \xi_6]^T = [1.0, 0.95, 1.0, 0.95, 0.95, 1.0]^T$. Although the control parameters in the comparative controllers are obtained under the condition that there is no variation between cylinders, it is reasonable and necessary to assess the control effect under the imbalance cylinder condition. Because the imbalance cylinder working ability would occur and be different with its original condition when the controller was designed due to varying dynamics and ageing of components of the fuel injection system [41].

From Figure 8: Zoom1 and Zoom3, it can be observed that in both the acceleration and deceleration processes, LADRC, NLADRC, and SADRC are better than PID in terms of the control performance in overshoot and settling time. Moreover, LADRC and SADRC present slight advantage in overshoot when compared with NLADRC. As shown in Figure 8: Zoom2, the steady-state speed fluctuation in NLADRC and SARDC is obviously smaller than that in LADRC, followed by PID. When synthetically considering the control effects in overshoot and steady-state speed fluctuation, it is apparent that SADRC is the best one during the speed tracking process.

4.2. Anti-Interference Ability under Mutation Load Disturbances. As mentioned in the section above, when the ship voyages in the sea, the load torque is affected by wave. The load conditions become complex for marine engine. Especially, when sea waves make the partial or total propeller out of water surface then drop into water again, the load of engine would change violently. Under the same simulation condition as mentioned above, we design three different mutation loads to validate the proposed control scheme.

As displayed in Figure 9(a), when the mutation load is large (100% full load), the speed variations and settling time in LADRC and SADRC are obviously smaller than those in NLADRC and PID. Unexpectedly, the settling time in NLADRC is the longest; it is even far inferior to that in the classical PID. When the mutation load becomes to medium degree (60% full load), as shown in Figure 9(b),

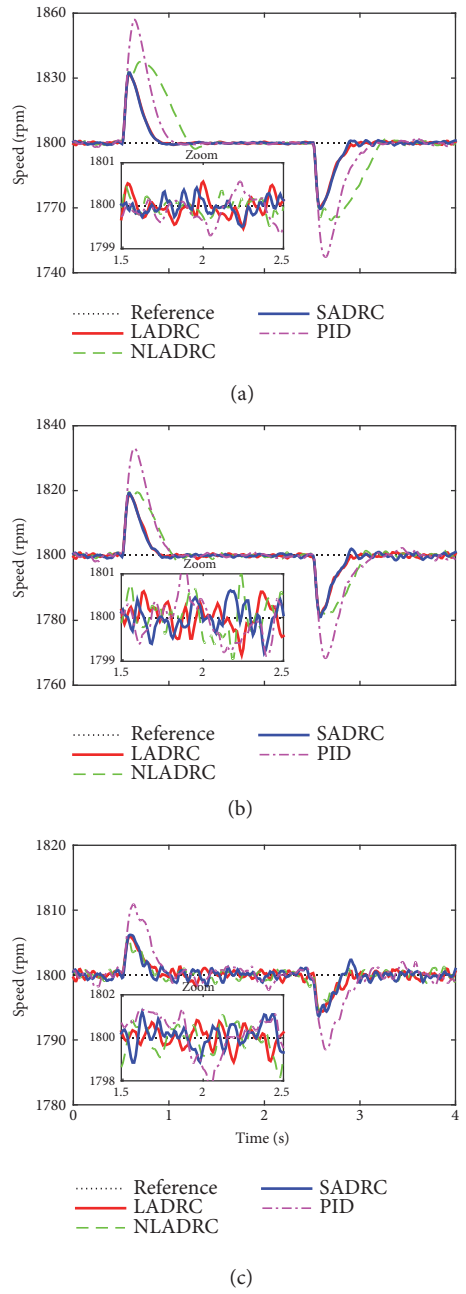

Figure 9: The speed responses under different levels of mutation load. (a) 100% full load. (b) 60% full load. (c) 20% full load.

the speed variations in LADRC, NLADRC, and SADRC are similar. Although the settling time in NLADRC catches up with that in PID, it is still not as good as that in the LADRC and SADRC. When the mutation load is small (20% full load), seen in Figure 9(c), both the speed variations and settling time in LADRC, NLADRC, and SADRC are almost the same. To understand well the impact of the extents of the load changing on the control performance of the comparative controllers, the estimate error of ESOs is compared in Figure 10. When the extents of load changing are larger (100% and 60% full load), the tracking error $e(k)$ in ESOs is far beyond the bound $[-1, 1]$ (see Figure 10, (a1, a2, a3, b1, b2, b3)), which results in performance deterioration for NLESO. This is the reason why the NLADRC shows bad control performance in such conditions. On the contrary, when the load change is smaller (20% full load), the tracking error $e(k)$ in ESOs is similar and within the bound $[-1, 1]$ (see Figure 10, (c1, c2, c3)); as a result, the speed deviation and settling time during such processes for the ADRC related controllers are almost the same.

Besides, the control effects of the steady states after unloading different loads (during the time from 1.5s to 2.5s) are enlarged in the corresponding subplot in Figure 9. It can be observed that only SADRC can consistently maintain the

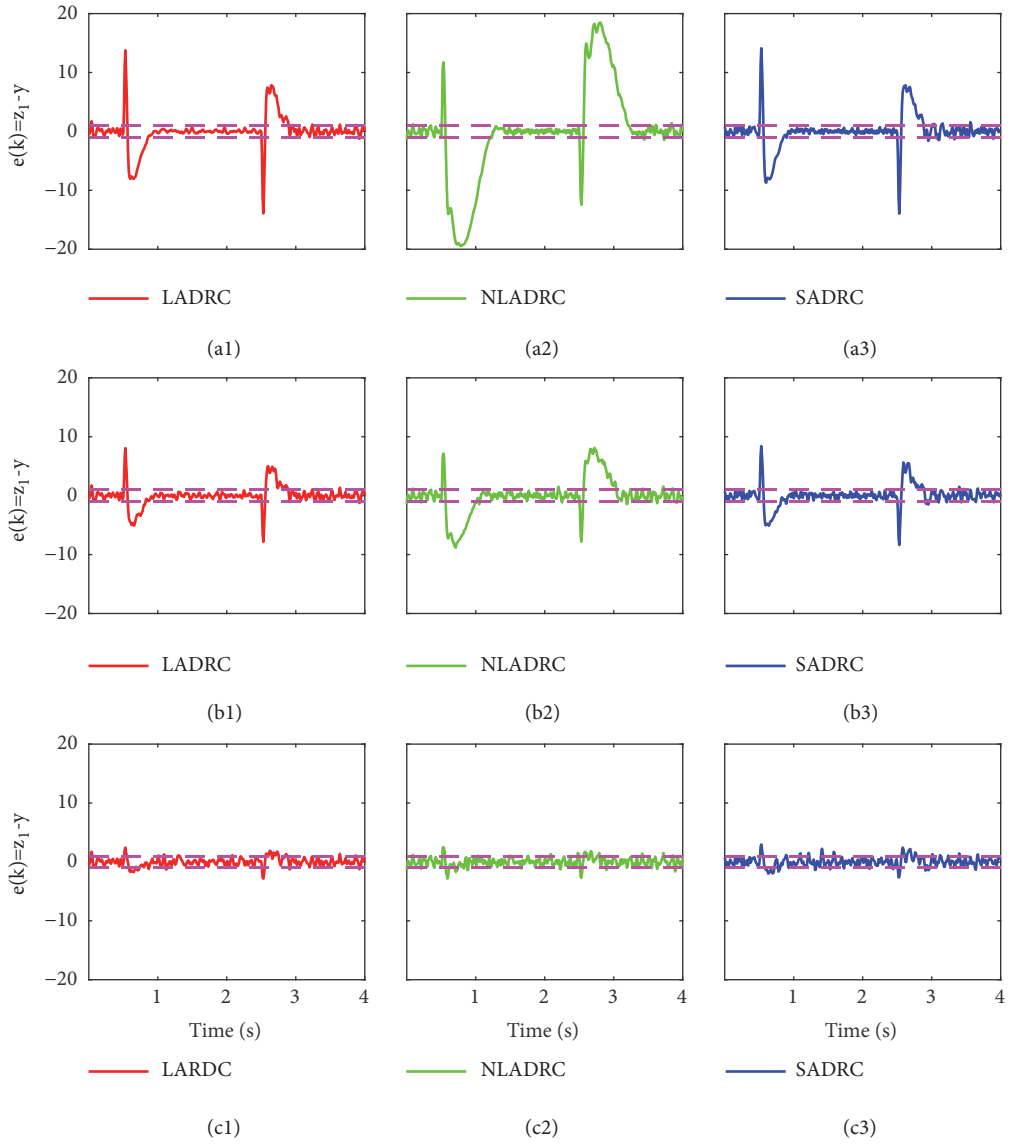

FIGURE 10: The tracking error $e(k)$ in ESOs under different levels of mutation load. (a1, a2, a3) 100% full load. (b1, b2, b3) 60% full load. (c1, c2, c3) 20% full load.

smallest speed fluctuation. To distinguish more clearly the control effect of the controllers under steady-state, the criteria in integral absolute error (*IAE*) of the system output and the total variation (*TV*) of the control signal are calculated. The *TV* index represents the manipulated input usage, which can be computed by (22), and detailed information can be found in [42–44].

$$\mathrm{TV} = \sum_{i=1}^{\infty} \left| u_{i+1} - u_i \right|, \tag{22}$$

where $[u_1, u_2, \ldots, u_i, \ldots]$ represents the discretized control input u.

Hence, a more detailed comparison in the criteria of *IAE* and *TV* for the three mentioned steady states is manifested in Table 1. It can be seen that the value of *IAE* in SADRC is significantly smaller than that in another three controllers, which means SADRC has better adaptability under steady-state after different levels of sudden load changing. As for the *TV* values, PID has less values in all the compared cases, which means that the control signal in PID is more smooth (as shown in Figure 11). From Figure 11, it can be observed that the control input in LADRC and SADRC adapts more quickly. On the one hand, it is similar to the explanation in [8] that faster antidisturbance ability is achieved by regulating the control input (fuel injection quality) quickly. On the other hand, it is also a drawback if high frequency oscillation with large amplitude occurs in control input. The existence of the inherent speed fluctuation and the imbalance working ability among cylinders are the main reason of such oscillation. From Table 1, we also know that, compared with LADRC, after unloading a larger load (100% and 60% full load), the

Table 1: The criteria of *IAE* and *TV* for different controllers after different mutation load processes.

	After unloading 100% full load				**After unloading 60% full load**				**After unloading 20% full load**			
	LADRC	NLADRC	SADRC	PID	LADRC	NLADRC	SADRC	PID	LADRC	NLADRC	SADRC	PID
IAE	0.193	0.148	0.136	0.241	0.241	0. 330	0.222	0.392	0.350	0.546	0.314	0.808
TV	65.3	59.5	58.8	12.1	96.7	88.2	90.9	21.7	141.5	140.6	138.2	31.1

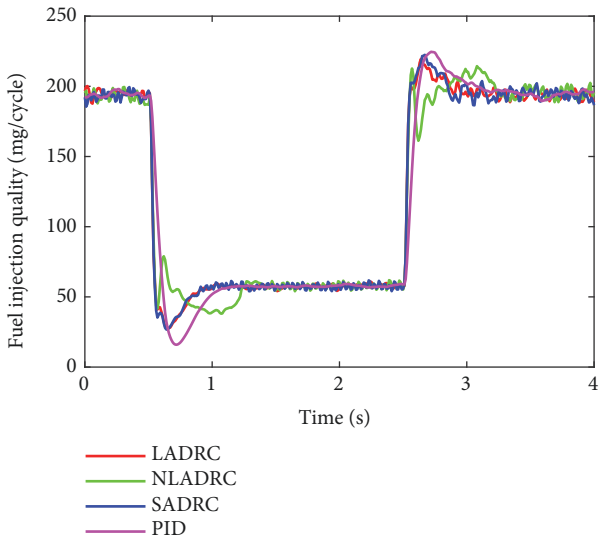

FIGURE 11: The comparison of control signal for the four controllers under mutation load (change 100% full load) condition.

TV values in SADRC have a reduction of about 10% to 6%. When after unloading a smaller load (20% full load), such reduction is unapparent. The reason is that the estimate error $e(k)$ starts to exceed the bound $[-1, 1]$ (as shown in Figure 10 (c1, c2, c3), during the time from 1.5s to 2.5s), resulting in the performance deterioration in NLESO. This is also the reason why the *IAE* value in NLADRC gets larger than that in LADRC and SADRC after unloading 20% full load.

In overall, SADRC maintains the same speed deviation as LADRC under load changing process, but smaller speed fluctuation and less oscillation in control signal under the steady-state after unloading process. Compared with NLADRC, SADRC has less settling time when the level of sudden load change is large and less speed fluctuation under steady-state after unloading. It can be concluded that SADRC has evident superiority to deal with the different degrees of sudden load change.

4.3. Anti-Interference Ability under Wave Load Disturbances. The wave load disturbance is another typical inevitable perturbation for marine engine. Considering the value of normalized load torque at 1800 rpm, three sine waves with different amplitudes are designed to represent different intensities of the wave load; the amplitudes are 100 N·m, 200 N·m, and 300 N·m, respectively. And the frequency is set to be 0.2 Hz.

Figure 12 gives the speed responses of the four controllers under the three different wave load disturbances. Intuitively, the speed fluctuation in PID is the largest among them. To show clearly the control performance in these controllers, the comparison in the indexes of *IAE* and *TV* are given in Table 2. When wave load is smaller (amplitude is 100 N·m or 200 N·m), the values of *IAE* for SADRC are the smallest among the four controllers. Inversely, the *IAE* values of the LADRC show significant disadvantage when wave load is larger than 100 N·m. Note that when wave amplitude is 300 N·m, the wave load disturbance reaches to a limiting case compared with the normalized load torque at 1800 rpm; hence, it can be concluded that the SADRC has the best performance in the index of *IAE* under different levels of possible wave disturbance. As for the index in *TV*, compared with the ADRC related controllers, the PID controller gains the smallest values. One reason is as mentioned above that the ADRC related controllers can react faster to the load disturbance, leading to the oscillation in control signal. By combing the NLADRC and LADRC, the *TV* values in SADRC have been reduced by 13%, 8%, and 10% under the three cases, respectively. From Figure 13, we know that, under different levels of wave load, the tracking error $e(k)$ in ESOs exceeds the bound $[-1, 1]$, especially when wave load is larger. With the switching scheme, the SADRC can combine the use of NLADRC and LADRC to obtain better control performance when the tracking error $e(k)$ in ESOs changes with the disturbance load. It can be regarded as an adaptation ability for SADRC.

5. Conclusions and Future Work

Among the previous ADRC related articles on the marine engine speed control, the impact of the intrinsical characteristics of the reciprocating engine on the control effect of ADRC is ignored. One important intention of this paper is to design an ADRC based controller for marine diesel engine with the consideration of the mentioned characteristics. To this end, a cycle-detailed hybrid nonlinear engine model which can simulate the inherent speed fluctuation is employed to evaluate the ADRC based controller.

Single LADRC or NLADRC is not enough to keep good control effect due to the strong nonlinearity, complex disturbance, and the extra inherent speed fluctuation in marine engines. The compound of LADRC and NLADRC is introduced to keep the merits of both methods. On the basis of the proposed engine model, the impact of the inherent speed fluctuation on the performance of the ESO is analyzed. Then the control parameters are adjusted with the consideration of such features for the proposed controller by modifying the previous approaches in the references. The proposed scheme is compared with LADRC, NLADRC, and well-tuned conventional PID via numerical simulations. The results indicate that the SADRC controller gains the advantages of both LADRC and NLADRC. It provides better control effect in speed tracking and also has preponderance in keeping better control performance under different levels of both mutation disturbance and wave disturbance. However, we also find that the control input oscillation in ADRC related controllers is stronger than that in PID under the proposed engine model.

As it is found that, for ADRC related approaches, the existence of inherent speed fluctuation and cylinder variations in reciprocating engines would affect its control performance, making the parameters tuning difficult and causing the oscillation in control input, our future work will be focused on studying the method to improve the control performance of ADRC for engine speed control and alleviate such oscillation. One possible way would be making use of filter method

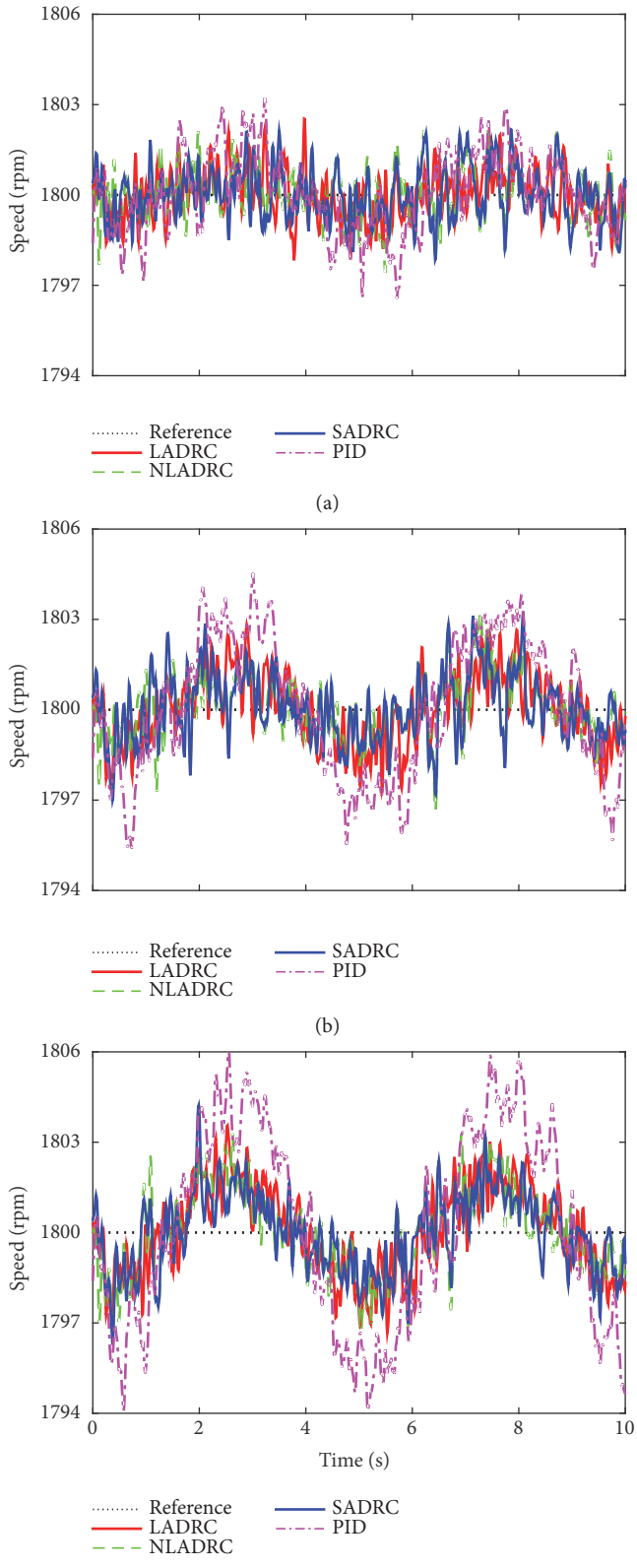

Figure 12: The speed responses under different levels of wave load. (a) Wave amplitude is 100 N·m. (b) Wave amplitude is 200 N·m. (c) Wave amplitude is 300 N·m.

Table 2: The indexes of *IAE* and *TV* for different controllers during different wave load conditions.

	Wave amplitude: 100 N·m				**Wave amplitude: 200 N·m**				**Wave amplitude: 300 N·m**			
	LADRC	NLADRC	SADRC	PID	LADRC	NLADRC	SADRC	PID	LADRC	NLADRC	SADRC	PID
IAE	6.2	6.4	5.9	11.3	9.3	8.0	7.9	20.1	12.8	10.3	10.4	28.1
TV	1546.2	1425.9	1349.1	379.5	1540.5	1431.2	1416.4	391.8	1612.5	1464.9	1444.4	469.9

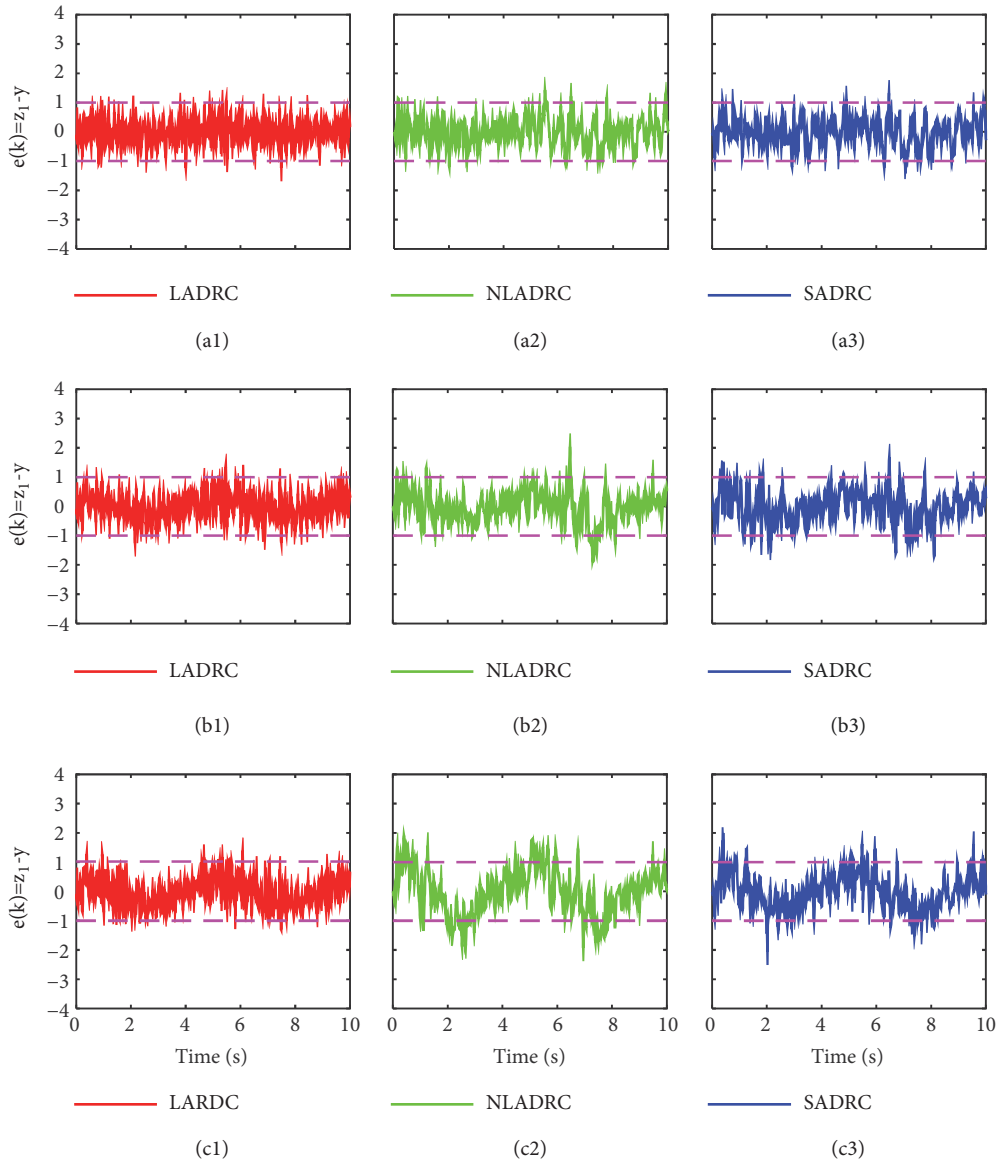

Figure 13: The tracking error $e(k)$ in ESOs under different levels of wave load. (a1, a2, a3) Wave amplitude: 100 N·m. (b1, b2, b3) Wave amplitude: 200 N·m. (c1, c2, c3) Wave amplitude: 300 N·m.

[45, 46]. The proposed method needs to be further verified on the real engine bench as well.

Data Availability

No data were used to support this study.

Conflicts of Interest

The authors declare no conflicts of interest.

References

[1] F. Di Natale and C. Carotenuto, "Particulate matter in marine diesel engines exhausts: Emissions and control strategies," *Transportation Research Part D: Transport and Environment*, vol. 40, pp. 166–191, 2015.

[2] N. Larbi and J. Bessrour, "Measurement and simulation of pollutant emissions from marine diesel combustion engine and their reduction by water injection," *Advances in Engineering Software*, vol. 41, no. 6, pp. 898–906, 2010.

[3] X. Li, Q. Ahmed, and G. Rizzoni, "Nonlinear robust control of marine diesel engine," *Journal of Marine Engineering Technology*, vol. 16, no. 1, p. 10, 2017.

[4] Y. Guo, W. Li, S. Yu et al., "Diesel engine torsional vibration control coupling with speed control system," *Mechanical Systems and Signal Processing*, vol. 94, pp. 1–13, 2017.

[5] R. Wang, X. Li, Y. Liu, W. Fu, S. Liu, and X. Ma, "Multiple Model Predictive Functional Control for Marine Diesel Engine," *Mathematical Problems in Engineering*, vol. 2018, Article ID 3252653, 20 pages, 2018.

[6] J. Wei, A. Zhang, D. Qin et al., "A coupling dynamics analysis method for a multistage planetary gear system," *Mechanism and Machine Theory*, vol. 110, pp. 27–49, 2017.

[7] C. Lynch, H. Hagras, and V. Callaghan, "Using uncertainty bounds in the design of an embedded real-time type-2 neuro-fuzzy speed controller for marine diesel engines," in *Proceedings of the IEEE International Conference on Fuzzy Systems*, pp. 1446–1453, Vancouver, Canada, July 2006.

[8] E. Kang, S. Hong, and M. Sunwoo, "Idle speed controller based on active disturbance rejection control in diesel engines," *International Journal of Automotive Technology*, vol. 17, no. 6, pp. 937–945, 2016.

[9] Z. Ye, "Modeling, identification, design, and implementation of nonlinear automotive idle speed control systems—an overview," *IEEE Transactions on Systems, Man, and Cybernetics, Part C: Applications and Reviews*, vol. 37, no. 6, pp. 1137–1151, 2007.

[10] N. I. Xiros, "PID marine engine speed regulation under full load conditions for sensitivity H∞-norm specifications against propeller disturbance," *Journal of Marine Engineering and Technology*, vol. 3, no. 2, pp. 3–11, 2004.

[11] G. Papalambrou and N. P. Kyrtatos, "H∞ robust control of marine diesel engine equipped with power-take-in system," in *Proceedings of the 11th IFAC Symposium on Control in Transportation Systems, CTS2006*, pp. 591–596, Netherlands, August 2006.

[12] T. Broomhead, C. Manzie, P. Hield, R. Shekhar, and M. Brear, "Economic model predictive control and applications for diesel generators," *IEEE Transactions on Control Systems Technology*, vol. 25, no. 2, pp. 388–400, 2017.

[13] Y. Yuan, M. Zhang, Y. Chen, and X. Mao, "Multi-sliding surface control for the speed regulation system of ship diesel engines," *Transactions of the Institute of Measurement and Control*, vol. 40, no. 1, pp. 22–34, 2018.

[14] O. Bondarenko and M. Kashiwagi, "Statistical consideration of propeller load fluctuation at racing condition in irregular waves," *Journal of Marine Science and Technology*, vol. 16, no. 4, pp. 402–410, 2011.

[15] S. Li and Z. Liu, "Adaptive speed control for permanent-magnet synchronous motor system with variations of load inertia," *IEEE Transactions on Industrial Electronics*, vol. 56, no. 8, pp. 3050–3059, 2009.

[16] H. P. Wang, D. Zheng, and Y. Tian, "High pressure common rail injection system modeling and control," *ISA Transactions®*, vol. 63, pp. 265–273, 2016.

[17] S. Li and J. Li, "Output Predictor-Based Active Disturbance Rejection Control for a Wind Energy Conversion System with PMSG," *IEEE Access*, vol. 5, pp. 5205–5214, 2017.

[18] Q. Zheng and Z. Gao, "Active disturbance rejection control: some recent experimental and industrial case studies," *Control Theory and Technology*, vol. 16, no. 4, pp. 301–313, 2018.

[19] W. Pan, H. Xiao, Y. Han, C. Wang, and G. Yang, "Nonlinear active disturbance rejection controller research of main engine for ship," in *Proceedings of the 2010 8th World Congress on Intelligent Control and Automation, WCICA 2010*, pp. 4978–4981, China, July 2010.

[20] H.-D. Hua, N. Ma, J. Ma, and X.-Y. Zhu, "Robust intelligent control design for marine diesel engine," *Journal of Shanghai Jiaotong University (Science)*, vol. 18, no. 6, pp. 660–666, 2013.

[21] A. W. Osburn and M. A. Franchek, "Reducing engine idle speed deviations using the internal model principle," *Journal of Dynamic Systems, Measurement, and Control*, vol. 128, no. 4, pp. 869–877, 2006.

[22] A. Balluchi, L. Benvenuti, M. D. D. I. Benedetto, S. Member, C. Pinello, and A. Luigi, "Automotive engine control and hybrid systems: Challenges and opportunities," *Proceedings of the IEEE*, vol. 88, no. 7, pp. 888–911, 2000.

[23] Z. Sun, "Tracking or rejecting rotational-angle dependent signals using time varying repetitive control," in *Proceedings of the 2004 American Control Conference (AAC)*, pp. 144–149, USA, July 2004.

[24] P. Li, T. Shen, and D. Liu, "Idle speed performance improvement via torque balancing control in ignition-event scale for SI engines with multi-cylinders," *International Journal of Engine Research*, vol. 13, no. 1, pp. 65–76, 2012.

[25] J. Karlsson and J. Fredriksson, "Cylinder-by-Cylinder Engine Models Vs Mean Value Engine Models for Use in Powertrain Control Applications," in *Proceedings of the International Congress & Exposition*.

[26] A. Balluchi, L. Benvenuti, L. Berardi et al., "Engine idle speed control via maximal safe set computation in the crank-angle domain," in *Proceedings of the 2002 IEEE International Symposium on Industrial Electronics, ISIE 2002*, pp. 618–622, Italy, July 2002.

[27] X. Li and S. Yurkovich, "Sliding mode control of delayed systems with application to engine idle speed control," *IEEE Transactions on Control Systems Technology*, vol. 9, no. 6, pp. 802–810, 2001.

[28] K. B. Goh, S. K. Spurgeon, and N. B. Jones, "Higher-order sliding mode control of a diesel generator set," *Proceedings of the Institution of Mechanical Engineers, Part I: Journal of Systems and Control Engineering*, vol. 217, no. 3, pp. 229–241, 2003.

[29] Tossaporn Chamsai, Piyoros Jirawattana, and Thana Radpukdee, "Robust Adaptive PID Controller for a Class of Uncertain Nonlinear Systems: An Application for Speed Tracking Control of an SI Engine," *Mathematical Problems in Engineering*, vol. 2015, Article ID 510738, 12 pages, 2015.

[30] Z. Gao, "Scaling and bandwidth-parameterization based controller tuning," in *Proceedings of the American Control Conference*, pp. 4989–4996, Denver, Colo, USA, June 2003.

[31] J. Li, Y. Xia, X. Qi, and Z. Gao, "On the Necessity, Scheme, and Basis of the Linear-Nonlinear Switching in Active Disturbance Rejection Control," *IEEE Transactions on Industrial Electronics*, vol. 64, no. 2, pp. 1425–1435, 2017.

[32] E. De Santis, M. D. Di Benedetto, and G. Pola, "Digital idle speed control of automotive engines: a safety problem for hybrid systems," *Nonlinear Analysis. Theory, Methods & Applications. An International Multidisciplinary Journal*, vol. 65, no. 9, pp. 1705–1724, 2006.

[33] C. Yang, X. Yang, and Y. Shardt, "An ADRC-Based Control Strategy for FRT Improvement of Wind Power Generation with a Doubly-Fed Induction Generator," *Energies*, vol. 11, no. 5, p. 1150, 2018.

[34] J. Q. Han, "From PID to active disturbance rejection control," *IEEE Transactions on Industrial Electronics*, vol. 56, no. 3, pp. 900–906, 2009.

[35] J. Han, *Active disturbance rejection control technique-the technique for estimating and compensating the uncertainties*, National Defense Industry Press, Beijing, China, 2008.

[36] Y. Q. Wang, G. Ren, and J. D. Zhang, "Anti-windup schemes for nonlinear active disturbance rejection control in marine steam turbine," *Journal of Marine Science and Technology-Taiwan*, vol. 24, no. 1, pp. 47–53, Feb 2016.

[37] X. Chen, D. H. Li, Z. Q. Gao, and C. F. Wang, "Tuning method for second-order active disturbance rejection control,"

in *Proceedings of the 30th Chinese Control Conference*, pp. 6322–6327, Yantai, China, 2011.

[38] Y. Huang and W. Xue, "Active disturbance rejection control: methodology and theoretical analysis," *ISA Transactions®*, vol. 53, no. 4, pp. 963–976, 2014.

[39] Y. X. Su, C. H. Zheng, and B. Y. Duan, "Automatic disturbances rejection controller for precise motion control of permanent-magnet synchronous motors," *IEEE Transactions on Industrial Electronics*, vol. 52, no. 3, pp. 814–823, 2005.

[40] J. Li, X.-H. Qi, Y.-Q. Xia, and Z.-Q. Gao, "On linear/nonlinear active disturbance rejection switching control," *Zidonghua Xuebao/Acta Automatica Sinica*, vol. 42, no. 2, pp. 202–212, 2016.

[41] F. Östman and H. T. Toivonen, "Adaptive cylinder balancing of internal combustion engines," *IEEE Transactions on Control Systems Technology*, vol. 19, no. 4, pp. 782–791, 2011.

[42] S. Skogestad, "Simple analytic rules for model reduction and PID controller tuning," *Journal of Process Control*, vol. 13, no. 4, pp. 291–309, 2003.

[43] M. Huba and I. Bélai, "Limits of a simplified controller design based on integral plus dead time models," *Proceedings of the Institution of Mechanical Engineers, Part I: Journal of Systems and Control Engineering*, 2018.

[44] M. Huba, "Performance measures, performance limits and optimal PI control for the IPDT plant," *Journal of Process Control*, vol. 23, no. 4, pp. 500–515, 2013.

[45] M. Huba and D. Vrančič, "Comparing filtered PI, PID and PIDD 2 control for the FOTD plants," *IFAC-PapersOnLine*, vol. 51, no. 4, pp. 954–959, 2018.

[46] M. Huba, P. Bistak, T. Huba, and D. Vrancic, "Comparing filtered PID and smith predictor control of a thermal plant," in *Proceedings of the 19th International Conference on Electrical Drives and Power Electronics, EDPE 2017*, pp. 324–329, Croatia, October 2017.